Ocean Engineering 183 (2019) 294–304

Contents lists available at ScienceDirect

Ocean Engineering

journal homepage: www.elsevier.com/locate/oceaneng

A noise impact assessment model for passive acoustic measurements of seabed gas fluxes

Jianghui Li[a,*], Paul R. White[a], Jonathan M. Bull[b], Timothy G. Leighton[a]

[a] Institute of Sound and Vibration Research, University of Southampton, Southampton, SO17 1BJ, UK
[b] Ocean and Earth Science, University of Southampton, National Oceanography Centre, Southampton, SO14 3ZH, UK

ARTICLE INFO

Keywords:
Acoustics
Ambient noise
Seabed gas flux
Carbon dioxide
Carbon capture and storage

ABSTRACT

Accurate determination of seabed gas flux is important for understanding natural processes as well as giving confidence that the size of any leaks from marine infrastructure can be properly assessed. Acoustic methods for flux determination require a relatively quiet underwater environment, and can fail when there is too much noise from other natural or anthropogenic sources. This study applies an acoustic monitoring example of seabed gas leakage in terms of sound level intensity, to statistically assess and minimize the impact from oceanic noise on seabed acoustic experiments which require a relative quiet environment. It addresses the question: how far from a source of radiated ambient noise does a recording hydrophone and location of seabed gas need to be so that acoustic methods for remotely determining gas flux are successful. We develop a model to assess impacts of ambient noise under various conditions, incorporating sound/noise sources (seabed gas leaks, sea surface agitation and shipping) and underwater acoustic propagation. The reliability of the model is tested by comparing measured seabed ambient noise in the central North Sea, and the robustness of it is verified by presenting statistical outliers and a receiver operating characteristic (ROC) curve. A range of scenarios are presented for several gas flow rates, which show the threshold of detection when the recording hydrophone is at different distances from the location of seabed gas escape, and competing noise sources (including shipping and surface waves).

1. Introduction

In the past decades, the increasing level of greenhouse gas, including carbon dioxide (CO_2) (Calleya et al., 2015), has resulted in global climate change as shown by a variety of observances, including by the melting of sea ice (Raynaud et al., 2000), the rise of sea level, and the disappearance of wetlands (Titus et al., 1991). For mitigating climate change caused by anthropogenic emissions of greenhouse gases, sub-seabed storage of CO_2 in Carbon Capture and Storage (CCS) facilities has been discussed as one of a range of technologies that could be used (Schmidt et al., 2015; Wang et al., 2016; Zhou and Wang, 2014; Winden et al., 2014). For the CCS to be successful, it is critical that the sequestered gas remains in the sub-surface and that any significant leakage is detected. In the marine environment there has been experimentation to determine the limits for this detection, as well as localization and quantification of CO_2 leakage from controlled sub-seabed gas release experiments (Blackford et al., 2014; Hvidevold et al., 2016; Berges et al., 2015; Atashwant et al., 2015; Taylor et al., 2015; Pearce et al., 2016). With regard to quantifying gas leakage using acoustic techniques, ambient noise is an essential factor that needs to be considered (Ainslie, 2010). Acoustic techniques are critically dependent on discrimination of bubble sounds from background noise to allow measurement of bubble radii and flux rates (Leighton and White, 2012).

In the ocean, ambient noise can be radiated from turbulence, surface wave agitation, thermal agitation, seismic events, rainfall, marine animals, ice sheet cracking, and shipping (Pizzuti et al., 2012; Hodges, 2011; Asolkar et al., 2017; Liu et al., 2005; Li et al., 2018; Brooker and Humphrey, 2016; Kellett et al., 2013; Wittekind and Schuster, 2016). The bubble source spectrum of interest for bubbles released from the seabed (where bubbles tend to be larger than those generated by breaking ocean waves) (Leighton et al., 2018; Brooks et al., 2009) is usually within a frequency band from hundreds of Hz up to around 25 kHz for small/moderate-sized injection points (Leighton and White, 2012; Leifer and Culling, 2010). The frequency band is particularly affected by ambient noise produced from the sea surface (Asolkar et al., 2017; Liu et al., 2005), as well as ship noise (Wenz, 1962; Rodney, 1990; Li et al., 2018; Brooker and Humphrey, 2016; Kellett et al., 2013). Noise outside this frequency band is usually not of concern

* Corresponding author.
E-mail address: J.Li@soton.ac.uk (J. Li).

https://doi.org/10.1016/j.oceaneng.2019.03.046
Received 11 September 2018; Received in revised form 5 March 2019; Accepted 29 March 2019
Available online 15 May 2019
0029-8018/

(Jensen et al., 2000). The interaction of the two types of noise sources and how they may affect the acoustic measurements, provides the impetus for this investigation. The approach taken here is to build a model to assess the impacts of ambient noise, by considering acoustic signals produced by oscillating bubbles as well as the noise received by the acoustic receiver.

Considering a prediction of acoustic carbon dioxide emission during a leak, Leighton and White (2012) described a method which provides quantitative measurements of gas leakage, which is applicable to a range of scenarios including from CCS facilities and natural methane seeps. In this initial study, the acoustic spreading loss is considered as spherical and more real propagation losses, e.g., with ray bending, are not considered, which is a simplification and unrealistic for remote acoustic detection. In an underwater environment, the effect of the seabed can be a potential problem, and is controlled by the sound speed profile (SSP) and physical characteristics of the sediment in the channel. The SSP and seabed parameters usually vary significantly at different field sites, which makes the sound propagation complicated and can be critical impact factor in underwater acoustics (Li and Zakharov, 2018; Li et al., 2016, 2017). For detecting bubble sounds, an acoustic receiver, e.g., a single omnidirectional hydrophone or an array of hydrophones, is usually employed. The position of the receiver relative to the centre of the gas seep is a critical factor when determining the performance of a system.

Sea surface generated noise is probably the most pervasive contributor to underwater noise in the ocean, particularly in areas affected by strong winds or in shallow water. Normally, the magnitude of the agitation noise is controlled by the strength of the wind blowing over the surface, causing breaking waves (Wenz, 1962) and entraining bubbles (Phelps and Leighton, 1998). The breaking waves then immediately radiate sound (Updegraff and Anderson, 1991; Lurton, 2010), such that the level of surface noise depends on the strength of the wind (Rodney, 1990). In underwater environments, ship noise is another significant contributor, which can cause substantial elevation of ambient noise (Wittekind and Schuster, 2016), and affects the ability to detect and quantify leaks. The ship noise, including transit noise and traffic noise (Kang et al., 2018), can be a dominant noise source, especially the transit noise, i.e., noise from a vessel travels in the vicinity of acoustic receiver, where there is little propagation loss in the acoustic channel (Jensen et al., 2000). To assess the impact of nearby shipping, we compute the distance at which a vessel is likely to hinder detection of a leak.

To determine whether detection of a leak is likely to occur, the signal-to-noise ratio (SNR) is calculated and compared to the Detection Threshold (DT). The value of DT incorporates the probability of detection (PD) and the probability of false alarm (PFA) (Dawe, 1997; Dunn et al., 2015). For example, for a PD of 50% and a PFA of 0.01% in Gaussian noise background, the DT is 6 dB (Dunn et al., 2015). The gas flow rate and the acoustic source level of the injected bubble are critical factors when determining the SNR. Leighton and White (2012) highlighted the lack of information on the source level, and that reliance on the literature and simple calculations to infer a source level was unsatisfactory and could lead to inaccuracies. The gas flow rate varies in different marine/laboratory experiments and natural seeps, and determines the intensity of the sound radiated by the bubbles (Vazquez et al., 2008; Manasseh et al., 2001). For example, the QICS (Quantifying and Monitoring Potential Ecosystem Impacts of Geological Carbon Storage) CO_2 release experiment (Blackford et al., 2014; Taylor et al., 2015; Atashwant et al., 2015) was carried out in Ardmuchnish Bay (10–12 m depth) with gas leakage rate estimated between approximately 0.1 and 18 L/min (Blackford et al., 2014). Laboratory experiments, such as (Thomanek et al., 2010), estimated leakage rates between 2 and 12 L/min. Further, numerous natural gas seeps have been discovered worldwide (Linke et al., 2014; Veloso et al., 2015; Thomanek et al., 2010; Leifer and MacDonald, 2003; Torres et al., 2002; Sauter et al., 2006; Sahling et al., 2009), and some of them were quantified from single seep vents: the reported leaks rates range from 0.1 L/min to 78 L/min.

In this paper, to assess the underwater ambient noise, particularly the ship noise, in light of the potential impacts to gas flux measurements, we develop a passive acoustic model. The bubble acoustic signal is predicted from the gas flow rate and the distribution of bubble sizes at the point of formation. The underwater sound propagation is simulated using the Bellhop ray-tracing program (Porter, 2011), to predict acoustic pressure field in ocean environments. In the modelling, we consider various conditions, involving underwater gas flow rates (0.5–18 L/min), wind speeds over the sea surface, ship noise source levels, ranges between acoustic receiver and gas seep centre (0.5–12 m), (nearby) ship distances to the receiver (0–5 km), and (distant) shipping density and distribution. A detection threshold of the receiver is applied to predict maximum hydrophone/bubble ranges and minimum ship/hydrophone distances. We take the central North Sea as an example of the modelled environment at a depth of 150 m.

This paper is organized as follows. Section 2 introduces the measurement scenario and model framework, while Section 3 describes the bubble sound simulator. Section 4 describes the ambient noise modelling, including noise radiated from sea surface agitation and shipping, and propagation loss in the acoustic propagation channel. Section 5 processes acoustic signals in the receiver. Section 6 displays simulation results, and Section 7 justifies the model with experimental data and statistical analysis. Section 8 completes the paper with concluding remarks, discussions, and gives outlooks for future work.

2. Measurement scenario and model framework

In underwater acoustic environments, a sound source having a Source Level (SL) subjected to propagation loss (PL), will have the following Spectral Receive Level (SRL) at the hydrophone:

$$\mathrm{SRL} = \mathrm{SL} - \mathrm{PL}. \tag{1}$$

The Source Level (SL) represents the sound radiated underwater by the source and is always referred to a standard range (1 m adopted here) from the acoustic centre of the source. The Source Level (SL) is expressed as a power density and measured in dB re 1 μPa^2/Hz at 1 m. The PL [dB] represents the power loss due to the propagation of the signal through the water column between the sound source and the hydrophone. Essentially, it is a function of two terms: the geometrical loss PL_g and the absorption loss PL_α:

$$\mathrm{PL} = \mathrm{PL}_g + \mathrm{PL}_\alpha. \tag{2}$$

The geometrical loss PL_g considers the geometrical spreading of sound wave, and the PL_α is the effect of absorption, both in the water column and seabed. In seeking to detect a gas leakage, we are concerned with both the sound made by the bubbles and the ambient noise (sea surface noise and ship noise), as shown in Fig. 1. The potential for the noise to mask the bubble sounds can be estimated based on the signal-to-noise ratio (SNR) (Urick, 2013):

$$\mathrm{SNR} = \mathrm{SPL}_b - \mathrm{NPL}, \tag{3}$$

where SNR is measured on a receive hydrophone expressed in dB, SRL_b is the SRL of the bubble signature, and NPL is the noise pressure level.

Fig. 2 shows the block diagram of the noise impact assessment simulator. In the simulator, there are blocks representing the bubble sound, ship transit and traffic noise and sea surface noise generators, propagation models, and hydrophone signal processing model.

3. Bubble sound simulator

As a bubble is released into the water column, it undergoes fluctuations in its volume which efficiently radiates sound (Leighton, 1994). The bubble acoustic signal, which is the sound of interest, is used for gas quantification at the receive hydrophone. At the

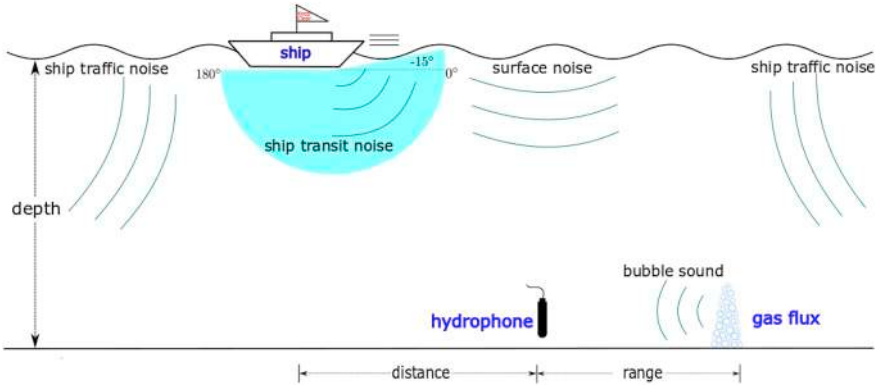

Fig. 1. Modelled gas flux measurement scenario. Noise is contributed from the sea surface and shipping. The model investigates the relative contributions of bubble emissions and ambient noise at different ranges/distances of the recording hydrophone from the sound sources.

hydrophone, the SRL of bubbles (SRL_b) can be expressed as:

$$SRL_b = SL_b - PL_b, \tag{4}$$

where SL_b is the bubble sound source level, depending on the bubble signal intensity in the frequency range of interest, and PL_b is the propagation loss associated with the bubble sound. The sound propagation in underwater acoustic environments are complicated and vary among different field sites in the ocean, then the propagation cannot be simply described as spherical or cylindrical propagation. Herein, the Bellhop program (Porter, 2011) is applied as the propagation model to calculate sound propagation loss in the channel. In the Bellhop calculation, we consider the rays combined coherently in a medium in the sense that the pressure signatures are summed (Hodges, 2011).

3.1. Bubble sound generator

To model the bubble sound generator, two steps are considered: the creation of probability density function (PDF) of bubble equilibrium radius, and the computation of approximate acoustic emission detected in the far field. This probability density function (PDF) is a statistical representation of the number of bubbles emitted per second as a function of radius.

3.1.1. Creating PDF of bubble equilibrium radius

We consider the probability density function (PDF) of the bubble radius as being approximated by a lognormal distribution (Lage and Esposito, 1999; Lehr et al., 2002; Orris and Nicholas, 2000; Leblond et al., 2014):

$$p_b^R = \frac{1}{R\sigma_l\sqrt{2\pi}} e^{(-(\ln R-\mu_l)^2/2\sigma_l^2)}, \tag{5}$$

where σ_l is the lognormal mean value [m], μ_l is the lognormal standard deviation [m], and R is the bubble radius [m]. With the bubble radius distribution p_b, the mean volume across the bubble population V_m (Yeh and Kwan, 1978) can be computed. Then, the average number of bubbles per second is given by:

$$N_b = V_r/V_m, \tag{6}$$

where V_r is the gas flow rate [m^3/s]. Note that the flow rate composes of components from both large bubbles and small bubbles. Through a large opening, the size of leaked bubble is larger than that from a small opening. The low pressure of large bubbles makes low ratio of $R_{\varepsilon 0i}/R_0$ (see Eq. (7)) corresponding to relative low frequency noise, while the high pressure of small bubbles makes high ratio of $R_{\varepsilon 0i}/R_0$ corresponding to relative high frequency noise.

3.1.2. Far field acoustic emission of the bubbles

Leighton and White (2012) identified the lack of a validated model for the source strength of a bubble emitted from a seabed as the major limitation in implementing their approach. Until an improved model becomes available, we will use their interim model to demonstrate the method. For a single bubble emitted from a leak, assume the bubble oscillates in a limit of small amplitude $|R_\varepsilon| \ll R_0$, which is valid for most ocean gas bubbles pulsating at their natural frequencies (Ainslie and

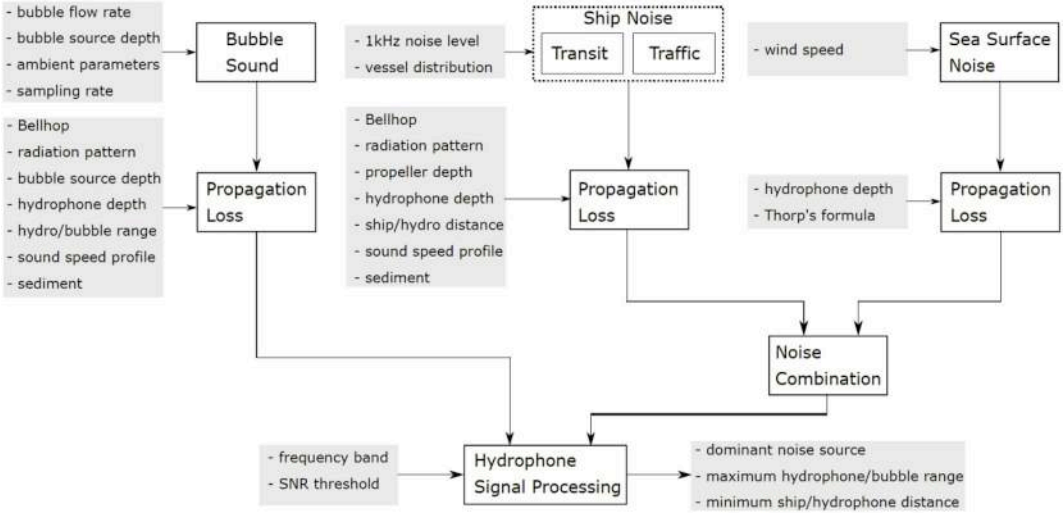

Fig. 2. Flowchart of the passive acoustic model, shows the dependencies in the integrated underwater noise impact assessment modelling approach.

Leighton, 2009). The oscillatory pressure signature in the liquid $P_{b1}(t)$ of the monopole emission detected at time t by a hydrophone in the far field for a single pulsating bubble, is given by (Leighton and White, 2012):

$$P_{b1}^{R_0}(t,\ t_i) = (\omega_0 R_0)^2 \frac{\rho_0}{r_1} R_{\varepsilon 0i} e^{-\omega_0 \delta_{tot}(t-t_i)/2} H(t-t_i)\cos\omega_0(t-t_i), \tag{7}$$

where R_0 is the bubble equilibrium radius [m], ρ_0 is the ambient liquid density [kg/m^3], $R_{\varepsilon 0i}$ is the initial bubble wall amplitude [m], δ_{tot} is the total dimensionless damping coefficient at bubble natural frequency (Leighton, 1994), t_i is the time at which the acoustic signal is first detected at the monitor, H is the Heaviside step function, and r_1 is the reference range (1 m adopted here) from the bubble acoustic centre. Low-amplitude pulsations occur at a natural angular frequency ω_0, which is given by (Leighton, 1994):

$$\omega_0 = \frac{1}{R_0\sqrt{\rho_0}}\sqrt{3\kappa\left(p_0 - p_v + \frac{2\sigma}{R_0}\right) - \frac{2\sigma}{R_0} + p_v - \frac{4\eta^2}{\rho_0 R_0^2}}, \tag{8}$$

where p_0 is the ambient pressure [Pa], p_v is the vapor pressure [Pa], σ is the surface tension [N/m], η is the shear viscosity [Pa.s], and κ is the ratio of specific heat of the gas at constant pressure to that at constant volume, depending on whether the gas is behaving adiabatically, isothermally, or in some intermediate manner (Siedler, 1986).

If the acoustic emissions of the bubbles are all uncorrelated, then the far-field acoustic signature of the bubble cloud (gas flux) can be expressed as

$$P_{b1}(t) = \sum_{i=1}^{N_b} P_{b1}^{R_0}(t,\ t_i),\quad t_i \in [0,\ T_b], \tag{9}$$

where t_i is randomly distributed in the interval [0 T_b], following the bubble radius probability density function PDF $p_b^{R_0}$.

3.2. Bubble sound propagation loss

A bubble can be regarded as omnidirectional source (Leighton and White, 2012), i.e., the power of it is equally radiated in all the directions. However, a lab experiment (Manasseh et al., 2004) has shown that for a vertical chain of rising bubbles the distribution of acoustic pressure around a bubble chain revealed a strong anisotropy in the acoustic field, and the sound appeared to propagate much more efficiently along the chain than normal to it. The Bellhop program that we are applying considers this anisotropy by defining the source beam pattern with angle-level pairs (Porter, 2011). In the calculation of PL_b, the hydrophone is situated at a range of r from the centre of the gas seep. The geometrical loss PL_g modelled as a spherical spreading from the centre of the gas seep to a reference range r_1, while the sound spreading from the reference range r_1 (1 m) to a sensor position $r \geq r_1$ are modelled using the Bellhop program with a SSP specific to the field site. The sound attenuation can be from spreading in the water column, scattering from the sea surface and seabed, and the absorption. The absorption loss PL_α in the water column, is related to the temperature, salinity, pH, frequency, the range of the hydrophone to receive acoustic signals, and the depth of the gas release field site. A variety of empirical relationships allowing the prediction of absorption have been proposed, e.g., in (Urick, 2013) and (Ochi et al., 2008), here we adopt the Thorp's formula presented as (Harris et al., 2007):

$$\alpha(f) = \frac{0.1f^2}{1+f^2} + \frac{40f^2}{4100+f^2} + 2.75\times 10^{-4} f^2 + 0.003, \tag{10}$$

where f is the frequency [kHz]. At the hydrophone position r, the received sound signals are from multipath, and the attenuation coefficient $\alpha(f)$ is applied to all the received multipath signals.

The propagation model estimates the propagation loss as a function of frequency $PL_b(\omega)$ between the range of $r_1 = 1$ m (the reference position for the source spectral level) and the hydrophone range r:

$$PL_b(\omega) = PL_{b(r)}(\omega) - PL_{b(r_1)}(\omega). \tag{11}$$

This is computed $\omega_{end}/\Delta\omega$ times for each ω value in the frequency band of interest [0 ω_{end}] with a frequency step $\Delta\omega$. Then, the calculated spectral shape $PL_b(\omega)$ is used to design a finite impulse response (FIR) filter within the frequency band [0 ω_{end}], and this filter is applied on the bubble sound pressure signal $P_{b1}(t)$. Allowing the time-domain bubble sound signal $P_{b(r)}(t)$ at the hydrophone position $r \geq r_1$ to be obtained.

4. Ambient noise simulator

The NPL in Eq. (3), is obtained by summing the contributions of the ambient noise, depending on the receiver bandwidth B and the overall noise spectral level (NSL) at the receiver. The noise spectral level (NSL) [dB re 1 μPa^2/Hz] is the power sum of the sound spectrum levels attributable to the predominant noise sources, and can be computed as:

$$NSL = 10\log_{10}\left(\sum_{q=1}^{Q} 10^{\frac{NSL_q}{10}}\right), \tag{12}$$

where Q is the number of noise sources considered within the bandwidth that contains major power of the bubble sound. In this paper, we consider three noise sources ($Q = 3$): the sea surface agitation noise ($q = 1$), the noise radiated from a single nearby vessel, i.e., ship transit noise ($q = 2$), and the noise radiated from vessels that are too far away to be heard individually (Bauer and Howlett, 1995), i.e., ship traffic noise ($q = 3$). Other noise sources, like turbulence noise (which dominates in the band 1–10 Hz) and thermal noise (dominant over 100 kHz) (Rodney, 1990), are secondary in the major bubble frequency band (usually between hundreds of Hz and couples of kHz). Each noise spectral level NSL_q is expressed as:

$$NSL_q = SL_q - PL_q,\ q = 1,...,Q, \tag{13}$$

where SL_q [dB re 1 μPa^2/Hz] is the source level radiated by the qth noise source and the PL_q [dB] is its corresponding propagation loss.

To obtain a time-domain sequence with the desired noise spectral level NSL_q, the following steps are taken. Firstly, a white Gaussian noise (WGN) signal $\mathbf{x} = [x(1),...,x(n),...,x(N)]$ is generated with N samples. Then, assign the spectral shape noise spectral level NSL_p on it by designing an FIR filter. Once the three noise sources, i.e., sea surface noise, ship transit noise and ship traffic noise, are generated, they are propagated into the underwater channel, which is simulated using the Bellhop program (Porter, 2011).

4.1. Sea surface noise

4.1.1. Surface noise source

The magnitude of the sea surface spectral level SL_l depends on the surface conditions and is governed by the wind speed. Empirical relationships between noise spectral level (NSL) and wind speed v_w [m/s] exist, one of which, valid in the 100 Hz-100 kHz range, is described by (Rodney, 1990):

$$SL_1(f) = 50 + 7.5\sqrt{v_w} + 20\log_{10}(f) - 40\log_{10}(f+0.4), \tag{14}$$

where f is the frequency [kHz].

4.1.2. Surface noise propagation loss

For the physical nature of the surface agitation, it is characterized by a distributed noise field. Neglecting reflections from the seabed, surface agitation generates a noise field which has a constant intensity at a given depth, d. However, the surface generated noise is affected by absorption as a function of depth (Buckingham, 1980; Chapman, 1983; Harrison, 1989), and can be approximated by:

$$PL_l(f) = \alpha(f) \times d, \tag{15}$$

where $\alpha(f)$ is the attenuation coefficient given by Eq. (10).

4.2. Ship transit noise

4.2.1. Transit noise source

Underwater noise radiated from a vessel passing nearby is also considered as an acoustic pollutant affecting passive acoustic measurement (Solan et al., 2016). The ship transit noise can be considered as being generated by a single nearby vessel with a number of different source mechanisms, e.g., water flow noise, auxiliary machinery and equipment noise, diesel generators noise, electric motors noise, and propeller noise.

For a vessel radiating underwater noise, an empirical equation, which considers the displacement, speed relative to cavitation inception speed, block coefficient as an indicator for wake field variations, mass of diesel engines and diesel engine resiliently mounted, can be taken to model the corresponding SL_2 (Wittekind, 2014):

$$SL_2(f) = 10\log_{10}(F_1 + F_2 + F_3), \tag{16}$$

where F_1 represents the low-frequency contribution, the F_2 represents the high-frequency propeller noise, and the F_3 represents the engine noise. The three terms are given by

$$F_1 = 2.2\times 10^{-10}f^5 - 2\times 10^{-7}f^4 + 6\times 10^{-5}f^3 - 8\times 10^{-3}f^2 + 0.35f + 125 + A + B, \tag{17a}$$

$$F_2 = -5\times\log(f) - \frac{1000}{f} + 10 + B + C, \tag{17b}$$

$$F_3 = 10^{-7}f^2 - 0.03f + 145 + D + E, \tag{17c}$$

where

$$A = 80\log_{10}\left(\left(\frac{v}{v_{CIS}}\right)\times 4c_B\right), \text{ speed \& block,} \tag{18a}$$

$$B = 10\log_{10}\left(\frac{\Delta}{\Delta_{ref}}\right)^{2/3}, \text{ displacement,} \tag{18b}$$

$$C = 60\log_{10}\left(\left(\frac{v}{v_{CIS}}\right)\times 1000\, c_B\right), \text{ speed \& block,} \tag{18c}$$

$$D = 15\log_{10}(m) + 10\log_{10}(n), \text{ engine mass \& number,} \tag{18d}$$

$$E = \begin{cases} 0, & \text{engine resiliently mounted} \\ 15, & \text{engine rigidly mounted} \end{cases}, \tag{18e}$$

In Eqs. (17) and (18), f [Hz] is the frequency of interest, v [knots] is the speed through water, v_{CIS} [knots] is the cavitation inception speed, c_B is the block coefficient, Δ[t] is the displacement, $\Delta_{ref} = 10{,}000$ t is the reference displacement, m [t] is the engine mass, and n is the number of engines operating at the same time. As Wittekind (Wittekind and Schuster, 2016) pointed out that the model is still continuously compared to most recent data and has been found reasonable and appropriate, we have adjusted the parameters in Eq. (17c) to fit the measured data, which will be discussed in Section 7.1.

4.2.2. Transit noise propagation loss

An assumption made is that the ship path takes the vessel directly over the top of the field site, so that the ship is always in the same vertical plane as the hydrophone. To predict the received level from a vessel at a distant point, it is important to take into account the directivity of ship noise. The noise radiated from a vessel is usually loudest approximately in angle range $\theta_{ship} \in [-15^o\ 180^o]$ (Bartle, 2003), as shown in Fig. 1.

The noise from a vessel is a local non-stationary noise source in the sense that the vessel radiates as a point-like dipole source, which changes its position dynamically, so that the relative distance between the vessel and the hydrophone changes as a function of time. For each position of the vessel, the propagation loss (PL_2) is computed using Bellhop, considering the effect of the seabed absorption and the multipath structure in the propagation channel.

4.3. Ship traffic noise

While one vessel is close to the hydrophone, other vessels are assumed distributed in the surrounding well-defined ocean area on the sea surface (Kang et al., 2018). The ship traffic noise (SL_3) accounts for the cumulative radiating effect of a number of vessels and corresponds to the distribution of these vessels. The ship traffic noise consists of a linear combination of radiated acoustic components from all these distributed vessels recorded by a hydrophone. For each acoustic component, the radiated source level is described by Eq. (16). The attenuation of the radiated noise (PL_3) from these vessels differs from the relatively large distances to the hydrophone. A more complete model would consider or estimate the statistics and geometries of surrounding vessels. For real-time marine traffic across the oceans, readers are referred to (Traffic, 2018).

5. Hydrophone signal processing

After the channel propagation of the four sound sources, the SNR at the hydrophone can be computed to estimate the potential for the noise to mask bubble sounds from gas release measurements. To decide whether a detection is made or not at the hydrophone, a SNR detection threshold [dB] is calculated. The process to determine a detection threshold depends on the PD and the PFA (Dunn et al., 2015). The relation between the SNR at the hydrophone output of the signal in Gaussian noise to the detection index is given by (Dawe, 1997):

$$DT = 5\log(\dot{d}/BT), \tag{19}$$

where B is the bandwidth, T is the integration time, and $\dot{d}$ is the detection index, which indicates how easy it is to observe a signal in noise. Urick (2013) presented receiver operating characteristic (ROC) curves for both the signal plus and noise as Gaussian probability density function PDF, from which we can find that for a PD of 50% and a PFA of 0.01%, the detection index is $\dot{d} = 16$, and the detection threshold = 6 dB. The value 6 dB is also imposed in (Leighton and White, 2012) as a detection threshold to determine maximum detection range.

6. Simulation results

As an example of the designed model for noise impact assessment, a set of scenarios of passive acoustic measurement of gas fluxes in the central North Sea are considered. Specifically, data from vicinity of the Goldeneye Complex (around 58°38′N, 01°08′E) is used (Fig. 3), which has been considered to be a possible site for CCS (Chadwick, 2015), and the depth of the seafloor is around 150 m (Shell, 2017). The shape of the sea surface is considered as sinusoidal waves, of which the height and period is affected by the wind speed. The seabed is considered as an acousto-elastic half space without layers, because of the high acoustic attenuation at the frequencies emitted by these bubbles (5–15 kHz, say) in the seabed surface layer (Leighton and Robb, 2008). In this part of the North Sea, the surface sediment is mostly mud (Stevenson et al., 1995; Paramor et al., 2009), below which is a sand layer, and so an attenuation coefficient of 0.7 dB/wavelength is appropriate (Porter, 1992).

In this scenario, the bubbles are generated at the seabed at 150 m water depth, and the sound radiates omnidirectionally. The sea surface noise is generated by the sea surface agitation, which radiates sound towards the seabed. The ship transit noise source is assumed to be generated at a depth of 2.5 m with a radiation angle interval from -15° (stern) to 180° (bow) (see Fig. 1), so as each component of the ship traffic noise. In the simulation, the SSP shown in Fig. 3 is applied. The simulated signals are constructed assuming an omnidirectional

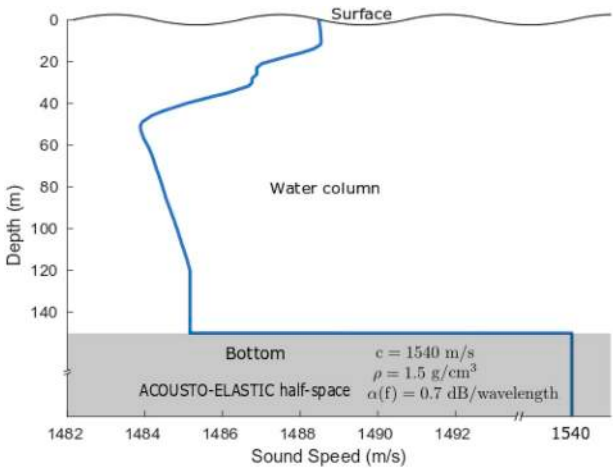

Fig. 3. Typical sound speed profile (SSP) at the Goldeneye Complex area of the North Sea at a water depth of 150 m. Seabed parameters (sound speed (c), density (ρ) and wavelength-dependent attenuation coefficient ($\alpha(f)$) in modelling are indicated.

Table 1
Parameters used in the simulations.

Parameter	symbol	value
seafloor depth		150 m
bubble source depth		150 m
gas flow rate		0.5–18 L/min
seafloor temperature		10°C
highest frequency of interest	ω_{end}	24 kHz
frequency step	$\Delta\omega$	24 kHz/1024
sea surface wind speed	υ_w	1 knot
ship noise source depth		2.5 m
ship noise radiation angle	θ_{ship}	[−15° 180°]
receiver(hydrophone) depth	d	149 m
receiver/bubble range	r	0.5–12 m
transit ship/receiver distance	D	0–5 km
traffic ship/receiver distance	$\hat{D}$	5–100 km
SNR detection threshold	DT	6 dB
duration of signal time series	T	1 s
sampling frequency	Fs	48 kHz

hydrophone, which is located close to the seafloor at depth $d = 149$ m. We simulate a variety of hydrophone ranges relative to the seep's centre, specifically a range r (0.5–12 m), and the focal vessel is modelled at horizontal distances D (0–5 km) from the position of the receive hydrophone. The parameters used in the simulations are shown in Table 1. During the simulation, no change in noise contribution from the sea surface and the vessel is assumed. Because of the randomness of the bubble radius generation and the ambient noise generation, 1000-time Monte Carlo simulation with the model has been conducted and the results averaged.

6.1. Bubble signals

We model possible gas leakage through the seabed, by bubble generation at the seafloor (150 m), with the bubble source spectral level [dB re 1 μPa^2/Hz] predicted at 1 m above the seabed. The default bubble flow rate is set to 4 L/min, which is a medium sized release experiment (Blackford et al., 2014; Thomanek et al., 2010). Note that the gas flux is measured as volume at depth, not at standard atmosphere. The parameters (ρ_0, p_0, p_v, σ, η, and κ) in Eq. (7) and Eq. (8) are based on those found in (Siedler, 1986). Fig. 4 shows the probability density function (PDF) of the bubble radius from the lognormal distribution Eq. (5) (number of bubbles generated per second per micron increment in radius range), from which we can see that the bubble radius mainly falls between 0.3 mm and 2.4 mm.

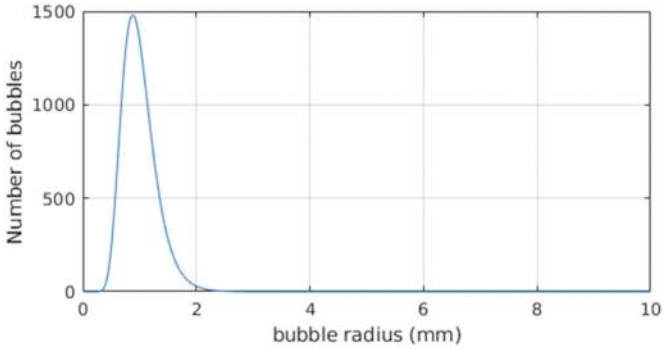

Fig. 4. Lognormal distribution of bubble radius used in the model.

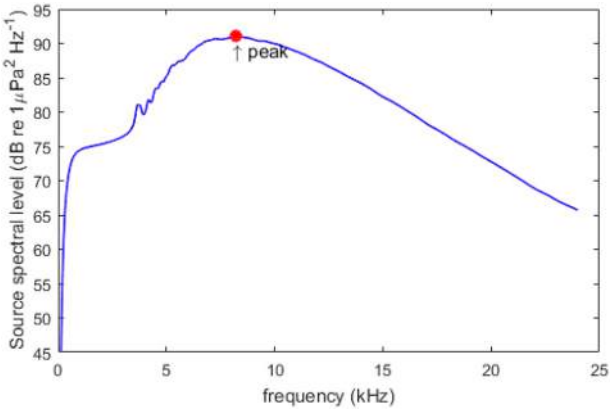

Fig. 5. Prediction of the source spectral level [dB re 1 μPa^2/Hz] at 1 m, assumed to occur at 150 m depth with bubble flow rate 4 L/min. The curve indicates the spectrum estimated from the theoretical model based on Eq. (9) (Leighton and White, 2012), with a peak value 91 dB re 1 μPa^2/Hz at 1 m (~8 kHz) as marked.

The curve, shown in Fig. 5, indicates the spectrum estimated from the theoretical model based on Eq. (9) (Leighton and White, 2012), considering ambient environment, including salinity, temperature, and the depth. Note that the curve may change depending on the changes of bubble sound time series and spectral methods. The maximum value of the bubble spectrum $SL_b = 91$ dB re 1 μPa^2/Hz is found at the frequency of around 8 kHz. Simulations demonstrated that 90% of the energy in the bubble spectrum lies between 5.3 and 14.8 kHz. The propagation loss of the bubble sound at 8 kHz is shown in Fig. 6(a).

6.2. Ambient noise

In the ocean, the frequency band of bubble radiation sound is particularly affected by ambient noise produced from the sea surface (Asolkar et al., 2017; Liu et al., 2005), ship transit noise and traffic noise (Wenz, 1962; Rodney, 1990; Li et al., 2018; Brooker and Humphrey, 2016; Kellett et al., 2013). Here we investigate the interaction of the three types of noise sources and how they may affect the acoustic measurements.

6.2.1. Sea surface noise

The sea surface noise source level SL_1 is computed from Eq. (14). To specify the noise spectral level NSL_1 shape, we consider a case of a relatively calm sea surface with wind speed at 1 knots, corresponding to the Sea State 1. The sea surface noise spectra, shown in Fig. 7(a), is obtained by filtering the generated Gaussian noise with the designed FIR filter by considering the position of an acoustic receive hydrophone, 1 m off the seabed here. Note that the propagation loss of sea surface

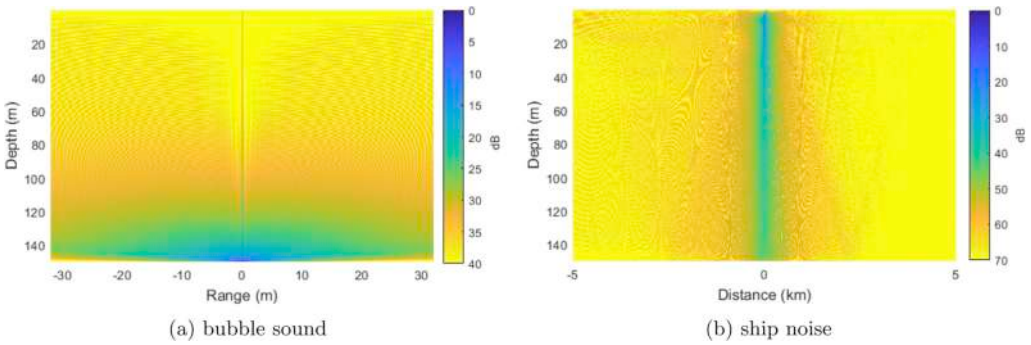

(a) bubble sound (b) ship noise

Fig. 6. Propagation loss (PL) [dB] of different sound sources in the channel at 8 kHz, calculated from the Bellhop program (Porter, 2011). The PL_b of bubble sound and the PL_2 of ship noise changes significantly as the hydrophone range/distance increases, compared to the PL_1 of surface noise as the hydrophone depth increases. The sound intensity reduces as the propagation loss increases. (a) Bubble sound PL_b. (b) Ship noise PL_2.

noise is relatively small in such shallow water, while the ship transit noise and traffic noise may experience much high propagation loss in the acoustic channel.

6.2.2. Ship transit noise

The ship transit noise is computed based on the RRS James Cook travelling at 14 knots in the central North Sea. Table 2 shows relevant parameters for the RRS James Cook. The channel propagation loss of the ship radiated noise at 8 kHz is shown in Fig. 6(b).

The ship transit noise spectra at distances 1–5 km, are shown in Fig. 7(c)-(e). It is seen that increasing the ship/hydrophone distance from 1 km to 3 km, the magnitude of the ship noise spectral level NSL_2 decreases by approximately 10–20 dB at 8 kHz. By comparing the noise spectral level (NSL) contribution of the sea surface agitation noise in

Table 2
Some characteristics of the ship 'James Cook'.

Characteristics	Values
Displacement	5800 t
Maximum speed	16.00 knots
Main propellers	2 × five – bladed inward turning
Propeller diameter	3.6 m
Propulsion plant	Diesel electric 2 × 2500 kW Teco dc mot (speed 0 to 180 rpm)
Power plant	4 × 1770 kW Wartsila 9L20 (1000 rpm generators, 9 cylinders) 2 × Siemens alternators, 60 Hz

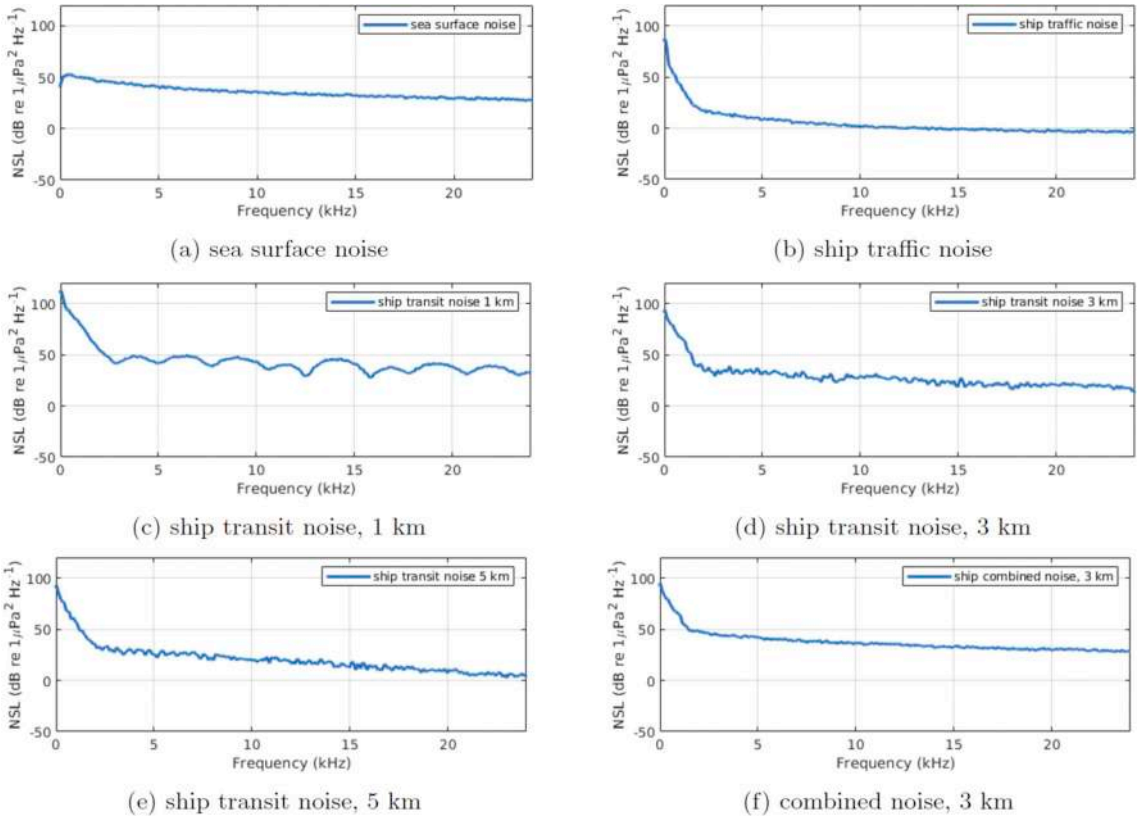

(a) sea surface noise (b) ship traffic noise

(c) ship transit noise, 1 km (d) ship transit noise, 3 km

(e) ship transit noise, 5 km (f) combined noise, 3 km

Fig. 7. Noise spectral levels (NSL) of sea surface noise at depth of 149 m and ship noise at distances of 1–5 km. The ship noise dominates the ambient noise at distances of 1 km, whereas the sea surface noise dominates the ambient noise at ship distances of 5 km. (a) Sea surface noise, 149 m depth. (b) Ship traffic noise. (c) Ship transit noise, 1 km. (d) Ship transit noise, 3 km. (e) Ship transit noise, 5 km. (f) Combined noise, surface + traffic + transit (3 km).

Fig. 7(a) and the ship noise in Fig. 7(c)-(e), we can see that the ship transit noise dominates the ambient noise field at distances less than 3 km, whereas the sea surface noise dominates at distances above 3 km. While ship transit noise is from specific ships nearby, the ship traffic noise is from all ship related noise sources in the vast ocean.

6.2.3. Ship traffic noise

The ship traffic noise is computed based on the distribution and types of distant vessels. Here we consider the noise sources with approximately equal engine powers and the vessels are considered equally distributed in the surrounding area. All vessels are assumed to have the same noise characteristics as the RRS James Cook travelling at 14 knots. According to the real-time ship tracker (Traffic, 2018), the minimum and maximum distances to the hydrophone are assumed to be $\hat{D}_{min}$ = 5 km and $\hat{D}_{max}$ = 100 km (distance to the nearest shore), and the number of vessels is estimated as 300 (average number of vessels within 100 km in the North Sea). The ship traffic noise experiences considerable propagation losses at such long distances, reducing the masking potential of the distant ship noise to the bubble sound at the hydrophone.

The ship traffic noise spectra level is shown in Fig. 7(b), agrees well with ship traffic noise measured and described in literature (Wenz, 1962; Bauer and Howlett, 1995). By comparing the noise spectral level (NSL) contribution of the sea surface agitation noise in Fig. 7(a) and the ship noise in Fig. 7(c)-(e), we can see that ship traffic noise dominates the ambient noise at low frequencies, as a rescue of significant attenuation of high frequency signals at long distances.

6.3. Impact assessment for gas flux measurement

The impacts of the ambient noise, combined by sea surface noise and ship noise, on gas flux measurement are assessed to calculate the SNR at the hydrophone as a function of frequency. These estimations are based on running the designed model simulation 1000 times and under the assumption that the hydrophone is placed at the same location (Li, 2017) as it would experience the same bubble sound and ambient noise levels at each time. Masking effects are here estimated from modelled ambient noise spectral levels and quantified as ship distance increases to fulfill the same detection threshold (6 dB).

Fig. 8 shows the smoothed SNR curves at different gas flow rates from 0.5 L/min to 18.0 L/min. In each case, different hydrophone/bubble ranges (0.5–12 m) determines the minimum ship/hydrophone distance required so that reliable estimates of gas flux can be made (the detection threshold shown as the black dashed line). In all these cases, the SNR is substantially elevated as the ship/hydrophone distance becomes less than 2.5 km. However, when the ship/hydrophone distance is increased to beyond 2.5 km, the SNR is nearly constant. This suggests that, the ship transit noise dominates as the vessel travels from 0 km to

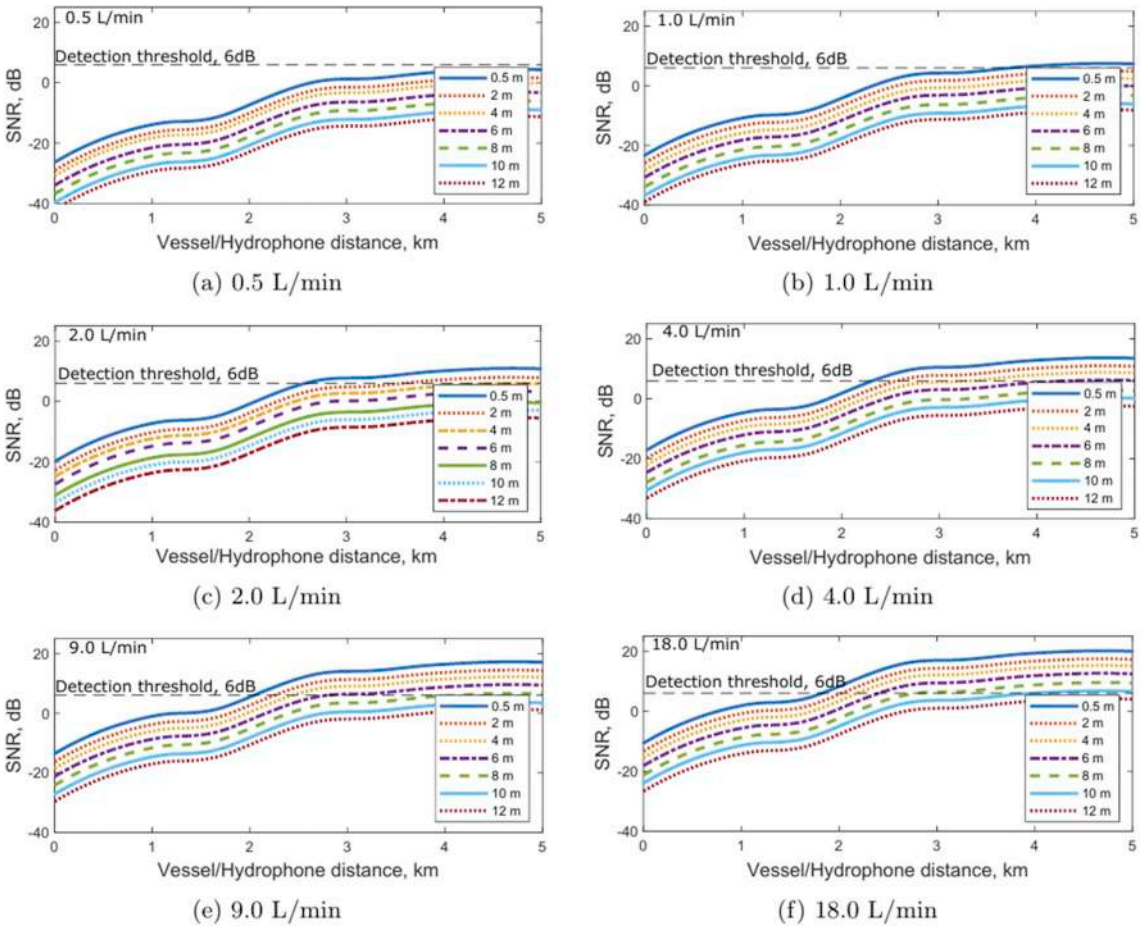

Fig. 8. Smoothed signal to noise ratio (SNR) for various seabed gas emission rates (0.5 L/min to 18.0 L/min) for different ranges (0.5–12 m) of the hydrophone from the centre of gas emissions (indicated as different color lines). The horizontal dashed line denotes the SNR detection threshold = 6 dB. When the colored SNR lines are above the detection threshold, the recording system (hydrophone) is able to detect the bubble sound radiated from the seabed gas emissions. (a) at 0.5 L/min the maximum hydrophone range is < 0.5 m. (b) at 1.0 L/min the maximum hydrophone range < 2 m. (c) at 2.0 L/min the maximum hydrophone range < 4 m. (d) at 4.0 L/min the maximum hydrophone range < 8 m. (e) at 9.0 L/min the maximum hydrophone range < 10 m. (f) at 18.0 L/min the maximum hydrophone range < 12 m. (For interpretation of the references to color in this figure legend, the reader is referred to the Web version of this article.)

2.5 km, while the sea surface noise and ship traffic noise dominate beyond this value. This also corresponds to the comparable noise levels shown in Fig. 7(a) and (d).

At the gas flow rate 0.5 L/min shown in Fig. 8(a), the hydrophone is unlikely to be able to detect the weak bubble sound due to background noise no matter how far away the vessel is. When the gas flow rate is increased to 1.0 L/min (Fig. 8(b)), the hydrophone is able to detect the bubble sound at 0.5 m when the ship is on greater than 3.7 km away. When the bubble flow rate is 4.0 L/min (Fig. 8(d)) and the hydrophone/bubble range is 2 m, the focal vessel only contaminates the measurements at distances less than 2.5 km. If the hydrophone is just able to detect the bubbles at a range of 6 m, while the ship distance is shortened by 0.5 km (increase of ship noise level), the hydrophone can compensate the SNR loss by moving 2 m towards the gas seep centre to improve the bubble signal spectral level. In the case of gas flow rate 18.0 L/min (Fig. 8(f)), due to the louder bubble sound, the vessel can be relatively close to the hydrophone.

The minimum ship/hydrophone distance, corresponding to an SNR equal to the detection threshold, can be determined from each of Fig. 8(b)-(f). Take Fig. 8(d) as an example, the minimum ship/hydrophone distance is close to 2.3 km when the hydrophone/bubble range is 0.5 m, while it has to be around 4.5 km when the hydrophone/bubble range is 6 m. This is limited by the hydrophone detection threshold (6 dB). If the hydrophone/bubble range is increased, the ship/hydrophone distances should also be increased, to keep the SNR higher than the detection threshold.

7. Experimental and statistical justification

To verify the effectiveness and robustness of the presented noise assessment model, we conducted field work in the central North Sea to measure the seafloor noise, and analyze the statistical outliers of the simulation results.

7.1. Comparison of noise measurement and model

The noise measurement experiment was conducted in the central North Sea (coordinate 58°38′73″N, 01°08′24″E) using the RRS James Cook in September 2017.

In the field work, an acoustic recorder with an absolutely calibrated hydrophone was attached on a lander mounted on the seafloor at depth 150 m. The hydrophone was 1 m above the seafloor. The measured noise data is compared with the modelled noise, in which case the wind speed over the sea surface was around 11 knots (Sea State 4), the ship speed was 14 knots, and the ship/hydrophone distance was around 5 km. The comparison result is shown in Fig. 9 using 1/3 octave bands.

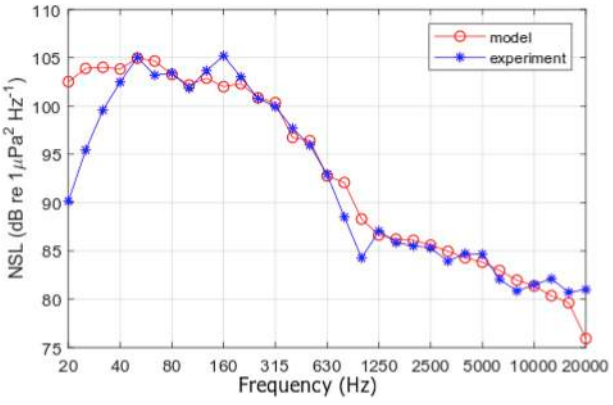

Fig. 9. Comparison of the modelled received noise level using the proposed/selected noise model (source level models + Bellhop propagation model) and measured noise level. The ship speed is 14 knots, and the wind speed is 11 knots.

Generally, there is good agreement between the modelled and observed noise levels, with a maximum noise at 40–80 Hz, typical of radiated noise from ships. Above these frequencies the level decreases by about 6 dB per octave until the surface agitation noise dominates at high frequencies. There is a band of strong tones measured at approximately 160 Hz caused by the tonal harmonics of the blade rates, which are, not shown in the model. Then at other frequency bands, the modelled level yields agreement within ± 5 dB compared to the measured data. Errors arise from simplifications in the models, and assumptions made when calculating propagation loss due to time-varying sound speed in the water column, unknown seabed bathymetry, and complex properties of the seabed. Our current experience indicates that the total error is a few dB, which is small, but it has to be accepted that the good or bad wake field, propeller design, and the non-stationary of the ship can also cause anomaly and no quantification of this has yet been made.

7.2. Statistical analysis

As the ambient noise and the bubble emission sound is non-stationarity, it is necessary to show the statistical outliers. In the 1000-time Monte Carlo simulations, the gas flow rate is set to 1.0 L/min, and the detection threshold is set to 6 dB. The simulation results are shown in Fig. 10. The PDF, smoothed using the kernel estimator, suggests that the distance threshold is distributed between 3400 m and 4100 m, centering at around 3740 m. Then, we use the kernel smoothing function to draw the receiver operating characteristic (ROC) curve, which shows the PFA. At the average distance threshold 3740 m, the PFA is about 50%. To be close to certain that underwater gas flux determination is successful, then the minimum ship/hydrophone distance should be 4100 m.

8. Conclusions and discussions

This study uses a numerical model to predict the dominant noise source, maximum bubble/hydrophone range, and minimum ship/hydrophone distance, for ensuring valid gas leakage detection and quantification from sub-seabed gas flux measurement in the field. The modelling results (Fig. 8) showed that the prediction is possible and can be applicable in a range of the marine acoustic environments. We have shown that the signal-to-noise ratio at an underwater acoustic recording system has been clearly modelled incorporating noise sources (sea surface agitation and shipping), bubble sound, and the acoustic propagation channel. The most important contribution of the modelling results is that it provides a statistical reference to avoid blind positioning of a ship radiating noise during passive acoustic measurements. The modelling work can be used as a guide to ensure that noise sources are sufficiently distant so that passive acoustic measurement of seabed gaseous emissions is possible and successful.

8.1. Variation of acoustic signatures

In the oceans, the acoustic signature can be affected by a variety of factors. Here we considered a relatively calm sea surface with wind speed $v_w = 1$ knots corresponding to Sea State 1. However, if the wind speed is higher than this level, reaching Sea State 4 or 5, it may produce significant breaking waves and can be the dominant noise source in a large area. The ship traffic noise can also be the dominant source when ship traffic is heavy.

The other important factor that cannot be ignored is the vessel specifications, such as size, speed, propulsion type, and load (McKenna et al., 2012, 2013). Besides the vessel characteristics, the acoustic signature at a given distance may also be influenced by interference patterns due to multiple radiation points from the ship, non-stationary of the ship, and multipath propagation such as the Lloyds' mirror effect (LME). Interference patterns vary according to the depth and distance

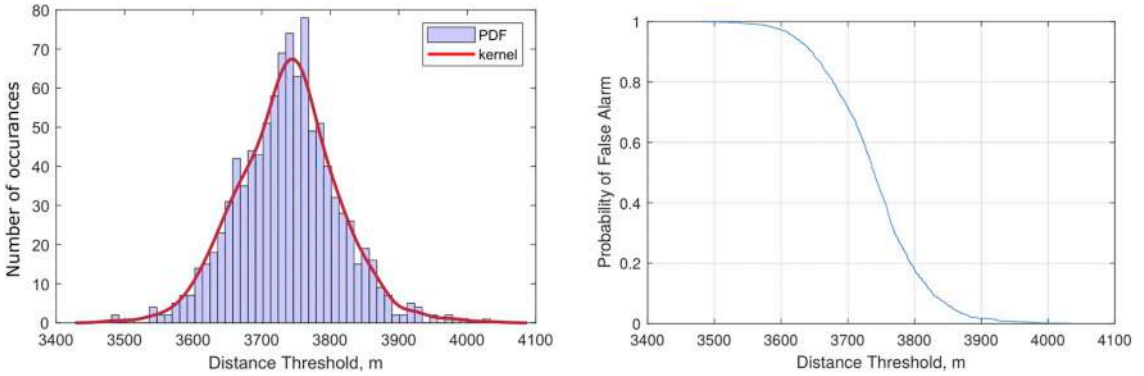

(a) Probability density function (PDF) (b) Receiver operating characteristic (ROC) curve

Fig. 10. Statistical outliers due to non-stationarity of the noise and bubble sound. (a) probability density function (PDF) of distance threshold with 1000 times Monte Carlo simulation. (b) Receiver operating characteristic (ROC) curve showing the probability of false alarm.

of source and hydrophone, bathymetry, sediment composition, the SSP, and the fact that the ship at close distance can no longer be considered as a point source (Hermannsen et al., 2014). The assessment results show pronounced variation in the simulations from actual source levels. Therefore, because of the complex propagation patterns, the noise levels around a nearby vessel, particularly in shallow water, are very difficult to predict (Hermannsen et al., 2014).

Furthermore, we paid attention only to noise radiated from a single vessel travelling close to the field site. However, once a number of ship transit noise sources, or self-generated noise from remotely operated underwater vehicle (ROV) or autonomous underwater vehicle (AUV) positioning a hydrophone near origin of the gas flux, the Gaussian noise model may not be valid to model the ship noise and the specific source statistics and geometries should be considered. Modelling of ship noise impacts, based on noise source levels and propagation models, depends heavily on the chosen vessel characteristics and environmental factors and should not solely be depended upon in noise impact assessments, but should be grounded in and verified by actual measurements (Hermannsen et al., 2014). In addition, in practice, to minimize noise interference, at least for the research vessels, all engines, generators, and echo sounders should be switched off or minimized during the gas flux measurements.

8.2. Outlooks for future work

As Leighton and White (2012) pointed out, until a good model for the bubble source level has been validated, particularly at depth, there remains uncertainty in the signal level and papers such as this can only address the noise component of the SNR. The presented noise impact assessment model can be used as a prediction bench mark and offer chance to investigate background noise in model scale at much lower cost and ultimately to reduce the probability of failure of the marine acoustic works, not only for the measurements of seabed gas fluxes, but also for wider underwater applications. Much more research in the related mechanisms is needed together with field measurement of the SNR such as on the seafloor of the central North Sea.

Acknowledgements

Funding for this work was provided by NERC grant NE/N01610/1 and the European Union's Horizon 2020 research and innovation programme under the grant agreement number 654462 (STEMM-CCS). We are grateful to Dr. Anna Lichtschlag for providing the sound speed profile collected at the Goldeneye Complex in the North Sea, as well as the Captain of the RRS James Cook and crew for enabling the scientific measurements at sea during JC152.

Data supporting this study (https://doi.org/10.5258/SOTON/D0861) are openly available from the University of Southampton repository.

Appendix A. Supplementary data

Supplementary data to this article can be found online at https://doi.org/10.1016/j.oceaneng.2019.03.046.

References

Ainslie, M.A., 2010. Principles of Sonar Performance Modelling. Springer, Victoria, pp. 55.
Ainslie, M.A., Leighton, T.G., 2009. Near resonant bubble acoustic cross-section corrections, including examples from oceanography, volcanology, and biomedical ultrasound. J. Acoust. Soc. Am. 126, 2163–2175.
Asolkar, P., Das, A., Gajre, S., Joshi, Y., 2017. Comprehensive correlation of ocean ambient noise with sea surface parameters. Ocean. Eng. 138, 170–178.
Atashwant, D., Tengberg, A., Aleynik, D., Fietzek, P., Shitashima, K., Lichtschlag, A., Hall, P.O., Stahl, H., 2015. Detection of CO2 leakage from a simulated sub-seabed storage site using three different types of pCO2 sensors. Int. J. Greenhouse Gas Control 38, 121–134.
Bartle, E., 1 Jan. 2003. The Choice of Appropriate Tools (Technologies), Procedures and Strategies Can Make the Difference between the Success and Failure of a Research Expedition. [Online]. Available: http://www.mar-eco.no/learning-zone/backgrounders/deepsea_research/mareco_teechnology.html.
Bauer, B.J., Howlett, T., 1995. Aerographer's Mate 1 & C, Pensacola. Navel Education and Training Professional Development and Technology Center.
Berges, B.J., Leighton, T.G., White, P.R., 2015. Passive acoustic quantification of gas fluxes during controlled gas release experiments. Int. J. Greenhouse Gas Control 38, 64–79.
Blackford, J., Stahl, H., Bull, J.M., Berges, B.J., Cevatoglu, M., Lichtschlag, A., Connelly, D., James, R.H., Kita, J., Long, D., 2014. Detection and impacts of leakage from sub-seafloor deep geological carbon dioxide storage. Nat. Clim. Change 4, 1011.
Brooker, A., Humphrey, V., 2016. Measurement of radiated underwater noise from a small research vessel in shallow water. Ocean. Eng. 120, 182–189.
Brooks, I.M., Yelland, M.J., Upstill-Goddard, R.C., Nightingale, P.D., Archer, S., d'Asaro, E., Beale, R., Beatty, C., Blomquist, B., Bloom, A.A., 2009. Physical exchanges at the air–sea interface: UK–SOLAS field measurements. Bull. Am. Meteorol. Soc. 90, 629–644.
Buckingham, M., 1980. A theoretical model of ambient noise in a low-loss, shallow water channel. J. Acoust. Soc. Am. 67, 1186–1192.
Calleya, J., Pawling, R., Greig, A., 2015. Ship impact model for technical assessment and selection of Carbon dioxide Reducing Technologies (CRTs). Ocean. Eng. 97, 82–89.
Chadwick, A., 2015. Review Confirms Goldeneye Storage Capability and Capacity. British Geological Survey, Nottingham.
Chapman, D.M., 1983. An improved Kirchhoff formula for reflection loss at a rough ocean surface at low grazing angles. J. Acoust. Soc. Am. 73, 520–527.
Dawe, R.L., 1997. Detection Threshold Modelling Explained. Defence Science and Technology Organisation Canberra, Australia.
Dunn, F., Hartmann, W., Campbell, D., Fletcher, N.H., 2015. Springer Handbook of Acoustics. Springer, New York, pp. 173–175.
Harris, I., Albert, F., Zorzi, M., 2007. Modeling the underwater acoustic channel in ns2. In: *The 2nd International Conference on Performance evaluation Methodologies and Tools*, Nantes.
Harrison, C., 1989. Ocean propagation models. Appl. Acoust. 27, 163–201.

Hermannsen, L., Beedholm, K., Tougaard, J., Madsen, P.T., 2014. High frequency components of ship noise in shallow water with a discussion of implications for harbor porpoises (Phocoena phocoena). J. Acoust. Soc. Am. 136, 1640–1653.
Hodges, R.P., 2011. Underwater Acoustics: Analysis, Design and Performance of Sonar. John Wiley & Sons, Waterford, pp. 127–141.
Hvidevold, H.K., Alendal, G., Johannessen, T., Ali, A., 2016. Survey strategies to quantify and optimize detecting probability of a CO2 seep in a varying marine environment. Environ. Model. Softw 83, 303–309.
Jensen, F.B., Kuperman, W.A., Porter, M.B., Schmidt, H., 2000. Computational Ocean Acoustics. Springer Science & Business Media, La Spezia.
Kang, L., Meng, Q., Liu, Q., 2018. Fundamental diagram of ship traffic in the Singapore strait. Ocean. Eng. 147, 340–354.
Kellett, P., Turan, O., Incecik, A., 2013. A study of numerical ship underwater noise prediction. Ocean. Eng. 66, 113–120.
Lage, P., Esposito, R., 1999. Experimental determination of bubble size distributions in bubble columns: prediction of mean bubble diameter and gas hold up. Powder Technol. 101, 142–150.
Leblond, I., Scalabrin, C., Berger, L., 2014. Acoustic monitoring of gas emissions from the seafloor. Part I: quantifying the volumetric flow of bubbles. Mar. Geophys. Res. 35, 191–210.
Lehr, F., Millies, M., Mewes, D., 2002. Bubble-Size distributions and flow fields in bubble columns. AIChE J. 48, 2426–2443.
Leifer, I., Culling, D., 2010. Formation of seep bubble plumes in the Coal Oil Point seep field. Geo Mar. Lett. 30, 339–353.
Leifer, I., MacDonald, I., 2003. Dynamics of the gas flux from shallow gas hydrate deposits: interaction between oily hydrate bubbles and the oceanic environment. Earth Planet. Sci. Lett. 210, 411–424.
Leighton, T.G., 1994. The Acoustic Bubble. Southampton: Academic Press, London.
Leighton, T.G., Robb, G., 2008. Preliminary mapping of void fractions and sound speeds in gassy marine sediments from subbottom profiles. J. Acoust. Soc. Am. 124, 313–320.
Leighton, T.G., White, P.R., 2012. Quantification of undersea gas leaks from carbon capture and storage facilities, from pipelines and from methane seeps, by their acoustic emissions. Proc. R. Soc. A 468, 485–510.
Leighton, T.G., Coles, D.G., Srokosz, M., White, P.R., Woolf, D.K., 2018. Asymmetric transfer of CO2 across a broken sea surface. Sci. Rep. 8, 8301.
Li, J., 2017. DOA tracking in time-varying underwater acoustic communication channels. MTS/IEEE OCEANS Aberdeen.
Li, J., Zakharov, Y.V., 2018. Efficient use of space-time clustering for underwater acoustic communications. IEEE J. Ocean. Eng. 43, 173–183.
Li, J., Liao, L., Zakharov, Y.V., 2016. Space-time cluster combining for UWA communications. MTS/IEEE OCEANS Shanghai.
Li, J., Zakharov, Y.V., Henson, B., 2017. Multibranch autocorrelation method for Doppler estimation in underwater acoustic channels. IEEE J. Ocean. Eng. 99, 1099–1113.
Li, D., Hallander, J., Johansson, T., 2018. Predicting underwater radiated noise of a full scale ship with model testing and numerical methods. Ocean. Eng. 161, 121–135.
Linke, P., Haeckel, M., Schneider, J. v., Vielstadte, L., Schmidt, M., Karstens, J., Berndt, C., Herreilers, H., Lichtschlag, A., James, R., 2014. Fluxes of CO2 from Natural Seep Sites and Sleipner Storage Site. GEOMAR: ECO2 Project Office.
Liu, J., Lin, I., Chu, C., 2005. Effects of sediment properties on surface-generated ambient noise in a shallow ocean. Ocean Eng. 32, 1887–1905.
Lurton, X., 2010. An Introduction to Underwater Acoustics: Principles and Applications. Springer, Praxis, pp. 23.
Manasseh, R., LaFontaine, R., Davy, J., Shepherd, I., Zhu, Y.-G., 2001. Passive acoustic bubble sizing in sparged systems. Exp. Fluid 30, 672–682.
Manasseh, R., Nikolovska, A., Ooi, A., Yoshida, S., 2004. Anisotropy in the sound field generated by a bubble chain. J. Sound Vib. 278, 807–823.
McKenna, M.F., Ross, D., Wiggins, S.M., Hildebrand, J.A., 2012. Underwater radiated noise from modern commercial ships. J. Acoust. Soc. Am. 131, 92–103.
McKenna, M.F., Wiggins, S.M., Hildebrand, J.A., 2013. Relationship between container ship underwater noise levels and ship design, operational and oceanographic conditions. Sci. Rep. 3, 1–49.
Ochi, H., Watanabe, Y., Shimura, T., 2008. Measurement of absorption loss at 80 kHz band for wideband underwater acoustic communication. Jpn. J. Appl. Phys. 47, 4366.
Orris, G.J., Nicholas, M., 2000. Collective oscillations of fresh and salt water bubble plumes. J. Acoust. Soc. Am. 107, 771–787.
Paramor, O., Allen, K., Aanesen, M., Armstrong, C., Hegland, T.J., Le Quesne, W., Piet, G., Raakjaer, J., Rogers, S., van Hal, R., 2009. MEFEPO: Making the European Fisheries Ecosystem Plan Operational: North Sea Atlas. University of Liverpool, Liverpool.
Pearce, J.M., Akhurst, M.C., Jones, D.J., Vincent, C.J., Booth, J.H., 2016. Pathways from pilot to demonstration: how can research advance CO2 geological storage deployment? British Geological Survey 35.
Phelps, A.D., Leighton, T.G., 1998. Oceanic bubble population measurements using a buoy-deployed combination frequency technique. IEEE J. Ocean. Eng. 23, 400–410.
Pizzuti, L., dos Santos Guimaraes, C., Iocca, E.G., de Carvalho, P.H.S., Martins, C.A., 2012. Continuous analysis of the acoustic marine noise: a graphic language approach. Ocean. Eng. 49, 56–65.
Porter, M.B., 1992. The KRAKEN Normal Mode Program. Navel Research Lab, Washington D.C.
Porter, M.B., 2011. "The Bellhop Manual and User's Guide: Preliminary Draft," Heat, Light, and Sound Research. Inc., La Jolla.
Raynaud, D., Barnola, J., Chappellaz, J., Blunier, T., Indermuhle, A., Stauffer, B., 2000. The ice record of greenhouse gases: a view in the context of future changes. Quat. Sci. Rev. 19, 9–17.
Rodney, F.C., 1990. Underwater Acoustic Systems. MacMillan Education Ltd., London.
Sahling, H., Bohrmann, G., Artemov, Y.G., Bahr, A., Bruning, M., Klapp, S.A., Klaucke, I., Kozlova, E., Nikolovska, A., Pape, T., 2009. Vodyanitskii mud volcano, Sorokin trough, Black Sea: geological characterization and quantification of gas bubble streams. Mar. Petrol. Geol. 26, 1799–1811.
Sauter, E.J., Muyakshin, S.I., Charlou, J.L., Schluter, M., Boetius, A., Jerosch, K., Damm, E., Foucher, J.-P., Klages, M., 2006. Methane discharge from a deep-sea submarine mud volcano into the upper water column by gas hydrate-coated methane bubbles. Earth Planet. Sci. Lett. 243, 354–365.
Schmidt, M., Linke, P., Sommer, S., Esser, D., Cherednichenko, S., 2015. Natural CO2 seeps offshore Panarea: a test site for subsea CO2 leak detection technology. Mar. Technol. Soc. J. 49, 19–30.
Shell, 12 Aug. 2017. Goldeneye Gas Platform, United Kingdom. [Online]. Available: http://www.offshore-technology.com/projects/goldeneye/.
Siedler, G.a.P.H., 1986. Properties of sea water. Oceanography 233–264.
Solan, M., Hauton, C., Godbold, J.A., Wood, C.L., Leighton, T.G., White, P.R., 2016. Anthropogenic sources of underwater sound can modify how sediment-dwelling invertebrates mediate ecosystem properties. Sci. Rep. 6, 20540.
Stevenson, A., Tait, B., Richardson, A., Smith, T., Nicolson, R., Stewart, H., 1995. The Geochemistry of Sea-Bed Sediments of the United Kingdom Continental Shelf: the North Sea, Hebrides and West Shetland Shelves, and the Malin-Hebrides Sea Area. British Geological Survey, Nottingham.
Taylor, P., Stahl, H., Vardy, M.E., Bull, J.M., Akhurst, M., Hauton, C., James, R.H., Lichtschlag, A., Long, D., Aleynik, D., 2015. A novel sub-seabed CO2 release experiment informing monitoring and impact assessment for geological carbon storage. Int. J. Greenhouse Gas Control 38, 3–17.
Thomanek, K., Zielinski, O., Sahling, H., Bohrmann, G., 2010. Automated gas bubble imaging at sea floor–a new method of in situ gas flux quantification. Ocean Sci. 6, 549–562.
Titus, J.G., Park, R.A., Leatherman, S.P., Weggel, J.R., Greene, M.S., Mausel, P.W., Brown, S., Gaunt, C., Trehan, M., Yohe, G., 1991. Greenhouse effect and sea level rise: the cost of holding back the sea. Coast. Manag. 19, 171–204.
Torres, M., McManus, J., Hammond, D., Angelis, M.D., Heeschen, K., Colbert, S., Tryon, M., Brown, K., Suess, E., 2002. Fluid and chemical fluxes in and out of sediments hosting methane hydrate deposits on Hydrate Ridge, OR, I: hydrological provinces. Earth Planet. Sci. Lett. 201, 525–540.
Marine Traffic. [Online]. Available: https://www.marinetraffic.com.
Updegraff, G.E., Anderson, V.C., 1991. Bubble noise and wavelet spills recorded 1 m below the ocean surface. J. Acoust. Soc. Am. 89, 2264–2279.
Urick, R.J., 2013. Principles of Underwater Sound, fourth ed. PENINSULA PUBLISHING, Washington.
Vazquez, A., Manasseh, R., Sanchez, R., Metcalfe, G., 2008. Experimental comparison between acoustic and pressure signals from a bubbling flow. Chem. Eng. Sci. 63, 5860–5869.
Veloso, M., Greinert, J., Mienert, J., Batist, M.D., 2015. A new methodology for quantifying bubble flow rates in deep water using splitbeam echosounders: examples from the Arctic offshore NW-Svalbard. Limnol Oceanogr. Methods 13, 267–287.
Wang, H., Zhou, P., Wang, Z., 2016. Experimental and numerical analysis on impacts of significant factors on carbon dioxide absorption efficiency in the carbon solidification process. Ocean. Eng. 113, 133–143.
Wenz, G.M., 1962. Acoustic ambient noise in the ocean: spectra and sources. J. Acoust. Soc. Am. 34, 1936–1956.
Winden, B., Chen, M., Okamoto, N., Kim, D.K., McCaig, E., Shenoi, A., Wilson, P., 2014. Investigation of offshore thermal power plant with carbon capture as an alternative to carbon dioxide transport. Ocean. Eng. 76 (1), 152–162.
Wittekind, D.K., 2014. A simple model for the underwater noise source level of ships. Journal of Ship production and design 30, 7–14.
Wittekind, D., Schuster, M., 2016. Propeller cavitation noise and background noise in the sea. Ocean. Eng. 120, 116–121.
Yeh, K., Kwan, K., 1978. A comparison of numerical integrating algorithms by trapezoidal, Lagrange, and spline approximation. J. Pharmacokinet. Pharmacodyn. 6, 79–98.
Zhou, P., Wang, H., 2014. Carbon capture and storage-Solidification and storage of carbon dioxide captured on ships. Ocean. Eng. 91, 172–180.